AGU ADVANCING EARTH AND SPACE SCIENCE

Geophysical Research Letters®

RESEARCH LETTER
10.1029/2021GL095242

Key Points:

- The observed Indian Ocean dipole (IOD)-El Niño-Southern Oscillation (ENSO) lead-lag relationship is primarily ENSO-driven, which adds no additional information to ENSO predictability
- The observed nonstationarity of inter-basin Pacific-Indian Ocean interannual connectivity is a manifestation of ENSO cycle complexity
- ENSO pacing regulates the IOD-ENSO relationship via changes in fundamental ENSO properties

Supporting Information:

Supporting Information may be found in the online version of this article.

Correspondence to:

W. Zhang,
zhangwj@nuist.edu.cn

Citation:

Jiang, F., Zhang, W., Jin, F.-F., Stuecker, M. F., & Allan, R. (2021). El Niño pacing orchestrates inter-basin Pacific-Indian Ocean interannual connections. *Geophysical Research Letters*, *48*, e2021GL095242. https://doi.org/10.1029/2021GL095242

Received 16 JUL 2021
Accepted 24 SEP 2021

El Niño Pacing Orchestrates Inter-Basin Pacific-Indian Ocean Interannual Connections

Feng Jiang[1], Wenjun Zhang[1], Fei-Fei Jin[2], Malte F. Stuecker[3], and Rob Allan[4]

[1]Key Laboratory of Meteorological Disaster of Ministry of Education (KLME), Nanjing University of Information Science and Technology, Nanjing, China, [2]Department of Atmospheric Sciences, School of Ocean and Earth Science and Technology (SOEST), University of Hawai'i at Mānoa, Honolulu, HI, USA, [3]Department of Oceanography and International Pacific Research Center (IPRC), School of Ocean and Earth Science and Technology (SOEST), University of Hawai'i at Mānoa, Honolulu, HI, USA, [4]Met Office Hadley Centre, Exeter, UK

Abstract El Niño-Southern Oscillation (ENSO), the primary source of year-to-year climate variability on Earth, has profound impacts on the Indian Ocean dipole (IOD), another important climate pattern. Much attention has been paid to potentially increased ENSO predictability by utilizing IOD conditions, inferred from a statistically significant correlation with ENSO at a long lead time. However, the intrinsic dynamics for the causality of this IOD-ENSO relationship remain largely elusive. Here, we demonstrate that the observed nonstationary IOD-ENSO lead-lag relationship is mainly ENSO-driven and therefore adds no additional information for ENSO predictability. The nonstationarity of their correlation is a manifestation of ENSO cycle complexity. Multi-climate model and theoretical results further demonstrate that ENSO pacing tightly controls the statistical IOD-ENSO relationship via changes in ENSO periodicity and regularity. This highlights that ENSO dominates the inter-basin Pacific-Indian Ocean interactions, shedding light on the key predictors for interannual pantropical climate variability.

Plain Language Summary Mounting attention has been paid to finding potential predictability sources outside the tropical Pacific to extend the prediction horizon of the El Niño-Southern Oscillation (ENSO). This study shows that the observed inter-basin lead-lag relationship in the Indo-Pacific, that was previously invoked to identify the Indian Ocean dipole as an independent predictor of ENSO, is in fact a manifestation of ENSO cycle complexity. We demonstrate that ENSO pacing tightly controls the inter-basin Pacific-Indian Ocean interannual relationship via changes in fundamental ENSO properties. The causal relationship identified here regarding inter-basin climate interactions is of crucial relevance for future studies investigating pantropical climate interactions.

1. Introduction

Back in 1974, the first seasonal climate prediction was issued, predicting an El Niño event in the next year based on an assumed persistence of the atmospheric component of the El Niño-Southern Oscillation (ENSO; Quinn, 1974), which even predated the understanding of many fundamental ENSO dynamics. The predicted El Niño did not occur as expected, however, it prompted the recognition that ENSO is the leading source of predictability in the global coupled ocean-atmosphere system (Cai et al., 2019; Latif et al., 1998; McPhaden et al., 2006; Wyrtki et al.,1976). Over the past few decades, the biggest step forward in our understanding of ENSO predictability is that ENSO events can be predicted up to three seasons in advance due to the slowly evolving heat content in the tropical Pacific upper ocean (Cane & Zebiak, 1985; Jin, 1997a, 1997b; Wrytki, 1975). Despite pronounced advances in ENSO theory and ENSO simulation in climate models, the effective predictive skill is still limited to three seasons due to the spring predictability barrier (Battisti, 1988; Webster & Yang, 1992). Counterintuitively, ENSO predictability has even decreased to only one season over the recent two decades (Hendon et al., 2009; McPhaden, 2012; Wang et al., 2010; Zebiak & Cane, 1987). Several studies have further revealed that sea surface temperature (SST) anomalies in other basins may also be involved in shaping ENSO evolution and that a better understanding of inter-basin interactions can be exploited advantageously to improve seasonal-to-interannual predictions (Cai et al., 2019; Wang, 2019). Particularly, Indian Ocean SST has been highlighted as a potential precursor candidate to increase ENSO prediction lead times (Kug & Kang, 2006; Kug et al., 2005; Izumo et al., 2010), considering the actively interconnected climate system in the Indo-Pacific domain.

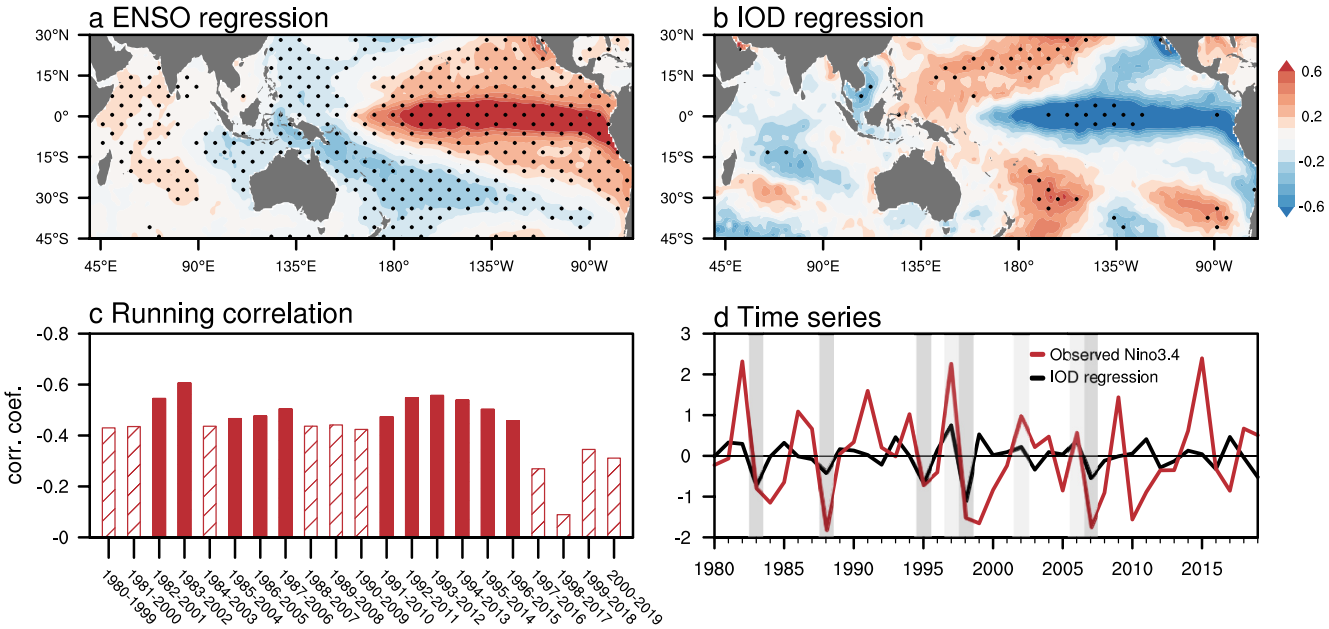

Figure 1. Relationships between El Niño-Southern Oscillation and Indian Ocean dipole (IOD). (a) Regression of boreal autumn (September–November) sea surface temperature (SST) anomalies (shading; °C) upon the ensuing winter (December–February) Niño3.4 index (defined as the SST anomaly averaged over 5°S–5°N, 120°–170°W). (b) Regression of boreal winter SST anomalies (shading; °C) upon the autumn DMI (defined as the SST anomaly difference between the western [10°S–10°N, 50°–70°E] and eastern Indian Ocean [10°S–0°, 90°E–110°E]) in the previous year. Dots in panels (a) and (b) indicate regression coefficients that are statistically significant at the 95% confidence level. (c) 20-year running correlation of the winter Niño3.4 index with the autumn DMI of the previous year. Solid bars indicate values exceeding the 95% confidence levels. (d) Observed (red line) and hindcasted (black line) Niño3.4 index (°C) using the autumn DMI of the previous year. Light and dark gray rectangles indicate the El Niño and La Niña years with a statistical IOD contribution accounting for more than 20%, respectively.

Typically, a developing El Niño can trigger a positive Indian Ocean dipole (IOD) event, characterized by positive SST anomalies in the western tropical Indian Ocean and negative SST anomalies along the Sumatra-Java coast (Figure 1a; Allan et al., 2001; Saji et al., 1999; Webster et al., 1999). The IOD peaks in boreal autumn and decays rapidly in the beginning of winter. As El Niño matures, a basin-scale warming develops in the Indian Ocean (IOBW; Xie et al., 2009; Yang et al., 2007), which usually peaks in boreal spring and persists into early summer. Recent studies suggested that interannual Indian Ocean climate variability, though largely driven by ENSO variability, might in turn feed back onto the ENSO evolution (Behera et al., 2006; Dommenget et al., 2006; Frauen & Dommenget, 2012; Jansen et al., 2009; Wu & Kirtman, 2004; Yu et al., 2002). Strong positive IOD events may induce anomalous westerlies in the western Pacific, conductive to El Niño development in the following month (Annamalai et al., 2010; Luo et al., 2010). During the El Niño decaying spring to summer, the IOBW-related easterly anomalies in the western Pacific, may in turn contribute to the rapid demise of the El Niño (Kug & Kang, 2006; Kug et al., 2005). However, the potential contribution of the Indian Ocean feedbacks to ENSO prediction might be limited, considering that these sources of the predictability are essentially originating from the ENSO cycle itself (Luo et al., 2010).

Different from the consensus on the ENSO predominance on the IOBW, considerable debate exists upon whether the IOD could be described as an intrinsic mode (Allan et al., 2001; Annamalai et al., 2003; Clarke & Van Gorder, 2003; Dommenget & Latif, 2002; Izumo et al., 2014; Kajtar et al., 2017; Saji et al., 1999; Stuecker et al., 2017; Sun et al., 2015; Yang et al., 2015). It is an issue of practical importance because an independent source of climate variability may provide additional potential information for ENSO prediction complementary to traditional effective predictors such as the Pacific warm water volume (Jin, 1997a; Meinen & McPhaden, 2000). In addition, recent studies indicate that the IOD has the potential to improve ENSO prediction beyond one year of lead time (Clarke & Van Gorder, 2003; Izumo et al., 2010, 2014). That is, a negative IOD event during boreal autumn tends to be followed by an El Niño formation in the winter of the following year (Figure 1b). This statistical lead relationship of IOD over ENSO, if confirmed, would provide a pathway to enhance ENSO predictability beyond its spring barrier. However, we find that the IOD

cannot be identified as an effective precursor for ENSO regardless of whether some feedback from IOD on ENSO exists, since the statistical IOD leading relationship over ENSO depends crucially on the ENSO cycle. Further investigation based on theoretical demonstration and climate model analyses shows that ENSO periodicity and cycle regularity are the key factors that control the statistical IOD-ENSO relationship. It highlights that ENSO dominates the inter-basin interaction between the tropical Pacific and Indian oceans on interannual timescales.

2. Data and Methods

2.1. Observations and Statistics

The monthly SST dataset utilized in this study is the global sea ice and SST analysis (1979–2019) from the Met Office Hadley Centre (HadISST version 1.1), which has a horizonal resolution of 1° × 1° (Rayner et al., 2003). Anomalies were computed by removing the monthly mean climatology over the period 1979–2019. The linear trend was removed to avoid possible influences related to global warming. The multi-taper method (MTM) with three tapers (Thomson, 1982) was used to confirm the rationality of the estimation for the ENSO period based on the autocorrelation structure (Figure S4 in Supporting Information S1). Statistical significance tests were performed based on the two-tailed Student's *t* test. ENSO events were defined according to the definition of the Climate Prediction Center based on a threshold of ±0.5°C of the Niño3.4 index (SST anomalies averaged over 5°S–5°N, 120°–170°W) for five consecutive months. Thirteen El Niño events (1982, 1986, 1987, 1991, 1994, 1997, 2002, 2004, 2006, 2009, 2015, 2018, and 2019) and 13 La Niña events (1983, 1984, 1988, 1995, 1998, 1999, 2000, 2005, 2008, 2010, 2011, 2016, and 2017) were identified.

2.2. Climate Models

Monthly SST output from the Phase 6 of the Coupled Model Inter-comparison Project (CMIP6) pre-industrial control (pi-control) simulations were utilized. Only one ensemble member was used for each model, mostly r1i1p1f1 with select models using ensemble member r1i1p1f2 based on availability. The last 100 years of 40 available model simulations were used for our analyses (see Table S1 in Supporting Information S1).

2.3. Theoretical RO ENSO-IOD Model

We consider a set of simultaneous equations including a simple recharge oscillator model (Chen & Jin, 2020; Jin, 1997a) for ENSO (Equations 1–3) and an ENSO-forced dynamical-statistical model (Hasselmann, 1976; Stuecker et al., 2017) for the IOD (Equation 4)

$$\frac{dT_E}{dt} = \left(R_0 - R_a \sin\left(\omega_a t - \varphi\right)\right) * T_E + \omega_0 * h_w + \sigma\xi\left[1 + B * H\left(T_E\right) * T_E\right] - cT_E{}^3 + bT_E^2, \quad (1)$$

$$\frac{dh_w}{dt} = -\varepsilon * h_w - \omega_0 * T_E, \quad (2)$$

$$\frac{d\xi}{dt} = -m * \xi + w, \quad (3)$$

$$\frac{dT_{\mathrm{IOD}}}{dt} = -\left(\lambda_0 + \lambda_D \cos\left(\omega_a t + \varphi_D\right)\right) * T_{\mathrm{IOD}} + \left(\alpha_0 + \alpha_A \cos\left(\omega_a t + \varphi_A\right)\right) * T_E, \quad (4)$$

In this framework, the RO model (Equation 1–3) describes the dynamic relationship between the ENSO-related SST anomalies (T_E) and the western equatorial Pacific thermocline anomalies (h_w). The RO ENSO time series (T_E) were then used to force the IOD model (Equation 4) to obtain the IOD time series. Details for the theoretical RO ENSO–IOD model and the estimated parameters are available in the Text S1 and Table S2 in Supporting Information S1.

3. Observed ENSO-IOD Relationship

We first revisit the observed lead-lag relationship between ENSO and IOD (Figure 1). A developing El Niño is usually accompanied by a positive IOD in boreal autumn (Figure 1a) and the positive IOD event tends to be followed by SST cooling in the central to eastern Pacific during the winter of the following year

(Figure 1b). Can we identify the IOD as a precursor for ENSO more than a year in advance based on statistical results? The conclusion should not be readily made, especially considering that the observed leading IOD-ENSO relationship is only marginally significant (Figure 1b) and highly variable in recent years (Figure 1c). If we consider the whole period as different samples with the same time span of 20 years, 10 out of 21 samples show a statistically insignificant correlation between IOD in autumn and following year ENSO conditions in winter. Their statistical relationship hovers at the 95% significance level until it collapses after the mid-2000s.

We here demonstrate that the statistical lead relationship of IOD over ENSO beyond one year only exists within the chain of ENSO events themselves (i.e., ENSO transition from El Niño to La Niña or vice versa). To quantify the possible IOD feedback on ENSO, we compare the observed and statistically hindcasted winter Niño3.4 index by using the autumn IOD of the previous year as a predictor (Figure 1d). The ENSO events in which the statistically hindcasted winter Niño3.4 amplitudes attain more than 20% of the observed amplitudes are defined as ENSO events with an apparent IOD contribution and eight events (three El Niño and five La Niña events) are identified. Note that the qualitative conclusion is not sensitive to the criterion of the percentage. Interestingly, for all ENSO events with an apparent IOD contribution, there are indeed opposite signed ENSO-related SST anomaly conditions in the tropical central to eastern Pacific during the previous winters (Figures 2a–2d). For the El Niño events with an apparent IOD contribution, the previous winter Pacific SST condition is manifested with significant cold SST anomalies in the eastern Pacific (Figure 2b). These La Niña events (Figure 2c) are similarly preconditioned with prominent positive SST anomalies over the central to eastern Pacific (Figure 2d). This result implies that the so-called contribution of previous autumn IOD to ENSO predictability originates from the previous ENSO conditions. In other words, we can also hindcast the Niño3.4 index by using the previous winter Niño3.4 index for these ENSO years with an apparent IOD contribution (red dots in Figures 2e and 2f). This dependence of the IOD contribution on the ENSO precondition is further evidenced by a particular case. During the second and third year of consecutive ENSO events, there exists a significant positive correlation between the current winter ENSO and the previous winter ENSO conditions (blue dots in Figure 2f). For these events, there even appears a significant positive correlation between the autumn IOD and winter ENSO of the next year (blue dots in Figure 2e). We emphasize that no evident IOD-ENSO relationship can be observed for other ENSO years. Therefore, we conclude that the observed statistical IOD-ENSO relationship is fully consistent with ENSO forcing IOD.

4. Multi-Climate Model Analyses and Theoretical Demonstration of the IOD-ENSO Relationship

Sampling issues due to the short observational record limits further insight into the IOD-ENSO relationship. Therefore, we examine the inter-basin IOD-ENSO relationship in 40 coupled models using the CMIP6 pi-control simulations (Table S1 in Supporting Information S1). Considering that the observed IOD-ENSO relationship beyond one year is tightly linked with ENSO preconditions in the previous winter, we approximately describe the ENSO cycle as winter ENSO lagged correlations by one year ($R_{\mathrm{ENSO(0)\&ENSO(1)}}$). The models exhibit a large diversity in ENSO cycle features (Figure 3a), which offers a chance to examine linkages of the ENSO cycle with the statistical lead relationship of IOD over ENSO. There is a significant inter-model relationship ($R = 0.70$, statistically significant at the 95% confidence level) between the simulated ENSO lagged correlation with itself ($R_{\mathrm{ENSO(0)\&ENSO(1)}}$) and the relationship between winter ENSO and autumn IOD in the previous year ($R_{\mathrm{IOD(0)\&ENSO(1)}}$) (Figure 3b). Based on the values of $R_{\mathrm{ENSO(0)\&ENSO(1)}}$, we select the five models with the highest negative correlation (blue bars in Figures 3a and 3c) and the five models with highest moderately positive correlation (red bars in Figures 3a and 3d). For the models that have the most negative ENSO lagged correlation, the IOD-ENSO lagged relationship exhibits a statistically significant IOD lead correlation over ENSO (Figure 3e). In contrast, the models without negative ENSO lagged relationship are not showing any long-lead signals of IOD before ENSO events in the previous year autumn (Figure 3f). These model results confirm that our observation-based conclusion that the so-called precursory IOD signal is dependent on the ENSO cycle.

It naturally comes to a question of how the ENSO cycle regulates the inter-basin IOD-ENSO relationship. To describe the general structure of the ENSO cycle, we show the autocorrelation of the observed Niño3.4 index as a function of lag months as a demonstration (Figure S1 in Supporting Information S1). The ENSO

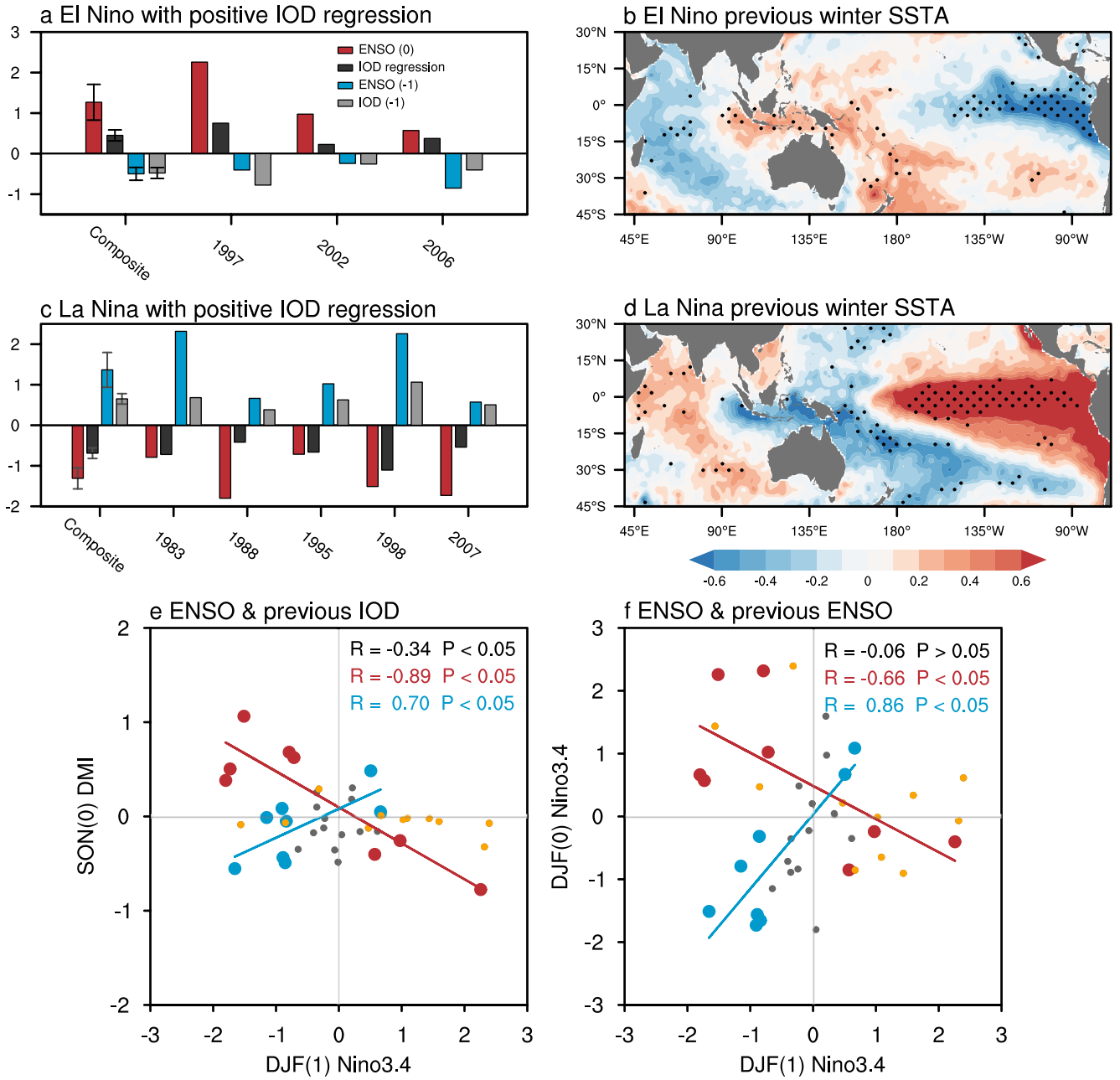

Figure 2. Observed statistical lead relationship of Indian Ocean dipole (IOD) over El Niño-Southern Oscillation (ENSO) dependent on the ENSO cycle. (a) El Niño events with an Indian Ocean dipole (IOD) contribution accounting for more than 20% and their composites with error bars corresponding to one standard deviation. Red bars denote the winter Niño3.4 index (°C), black bars the statistical IOD contribution (°C), blue bars the winter Niño3.4 index (°C) of the previous year, and gray bars the autumn DMI (°C) of the previous year. (b) Composite SST anomaly (°C) pattern in the previous winter during these El Niño events. Panels (c) and (d) are the same as panels (a) and (b) except for La Niña events. Dots in panels (b) and (d) indicate regression coefficients that are statistically significant at the 95% confidence level. Scatterplot of boreal winter Niño3.4 index against (e) Autumn DMI and (f) Winter Niño3.4 index of the previous year. Red dots in panels (e) and (f) denote the ENSO years with IOD contribution accounting for more than 20%, blue dots the consecutive ENSO years, orange dots the other ENSO years, and gray dots denote the residual years. The linear fits for the red and blue dots are displayed together with the corresponding correlation coefficients *R* and *P* values. The correlation coefficient (*R*; black) and *P* values for all dots is also shown.

cycle feature is mainly determined by two factors: the time distance of the maximum negative autocorrelation (defined as ENSO periodicity) and the correlation coefficient distance between the maximum positive and negative autocorrelation (defined as ENSO regularity). Since the maximum positive autocorrelation coefficient is a constant with the value of 1, we here used the absolute value of the maximum negative

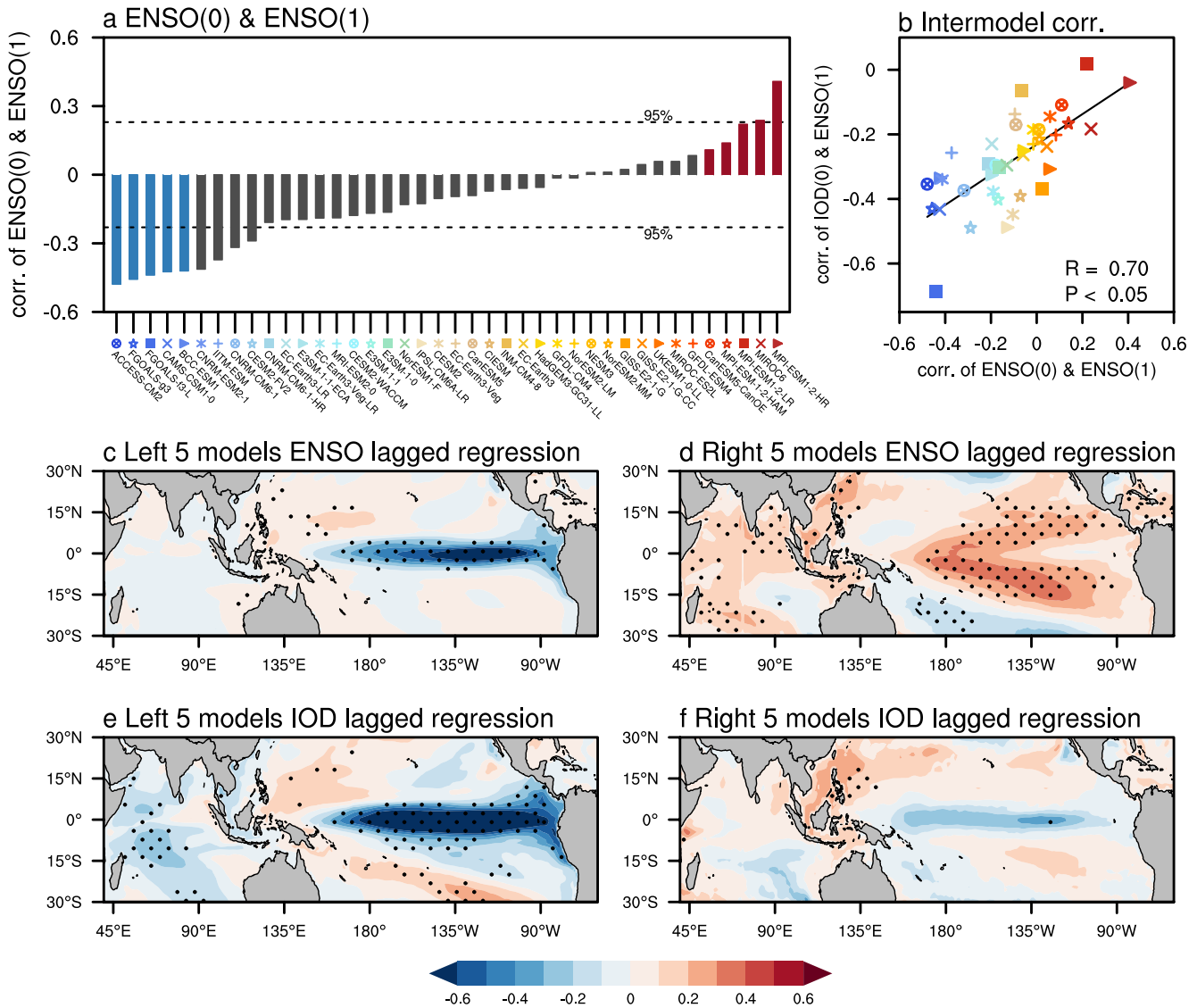

Figure 3. Phase relationship of Indian Ocean dipole (IOD) with El Niño–Southern Oscillation (ENSO) in pi-control climate simulations. (a) Correlation of boreal winter Niño3.4 index with the following winter Niño3.4 index for 40 CMIP6 models. The models are ranked by the correlation coefficients in an ascending order. (b) Scatterplot of $R_{\mathrm{ENSO(0)\ \&\ ENSO(1)}}$ (the correlation coefficient between the winter Niño3.4 index and the following winter Niño3.4 index) and $R_{\mathrm{IOD(0)\ \&\ ENSO(1)}}$ (the correlation between the autumn DMI and the winter Niño3.4 index of the following year). The linear fit (solid black) is displayed together with the correlation coefficient *R* and *P* values. The gray dashed lines denote the observations for reference. (c) Composite of the regressed winter SST anomalies (°C) upon the previous winter Niño3.4 index for the leftmost five models with the most negative correlation coefficients (models indicated by blue bars in panel (a)) and (d) the rightmost five models with the most positive correlation coefficients (models indicated by red bars in panel (a)). Panels (e) and (f) are the same as panels (c) and (d) except for the regressed winter SST anomalies (°C) upon the autumn DMI of the previous year.

autocorrelation coefficient to measure the ENSO regularity change. We construct a conceptual ENSO-IOD framework involving the ENSO recharge oscillator (RO) model (Chen & Jin, 2020; Jin, 1997a) and an ENSO-forced IOD dynamical-statistical model (Stuecker et al., 2017; Zhao et al., 2019, 2020) The ENSO period and its cycle regularity are determined by the critical parameter that controls the fundamental properties of the RO ENSO (Chen & Jin, 2020). The theoretical model (see Section 2) results show that the statistical lead relationship of IOD over ENSO ($R_{\mathrm{IOD(0)\&ENSO(1)}}$) is strengthened as the ENSO period is shortened and its cycle becomes more regular in a basically linear manner (gray dots in right side of Figure 4a). Importantly, the observed statistical lead relationship of IOD over ENSO can be realistically reproduced if we set the ENSO period and its cycle regularity to the observed value in the theoretical RO ENSO-IOD model, in which any feedback from IOD to ENSO is not allowed by design.

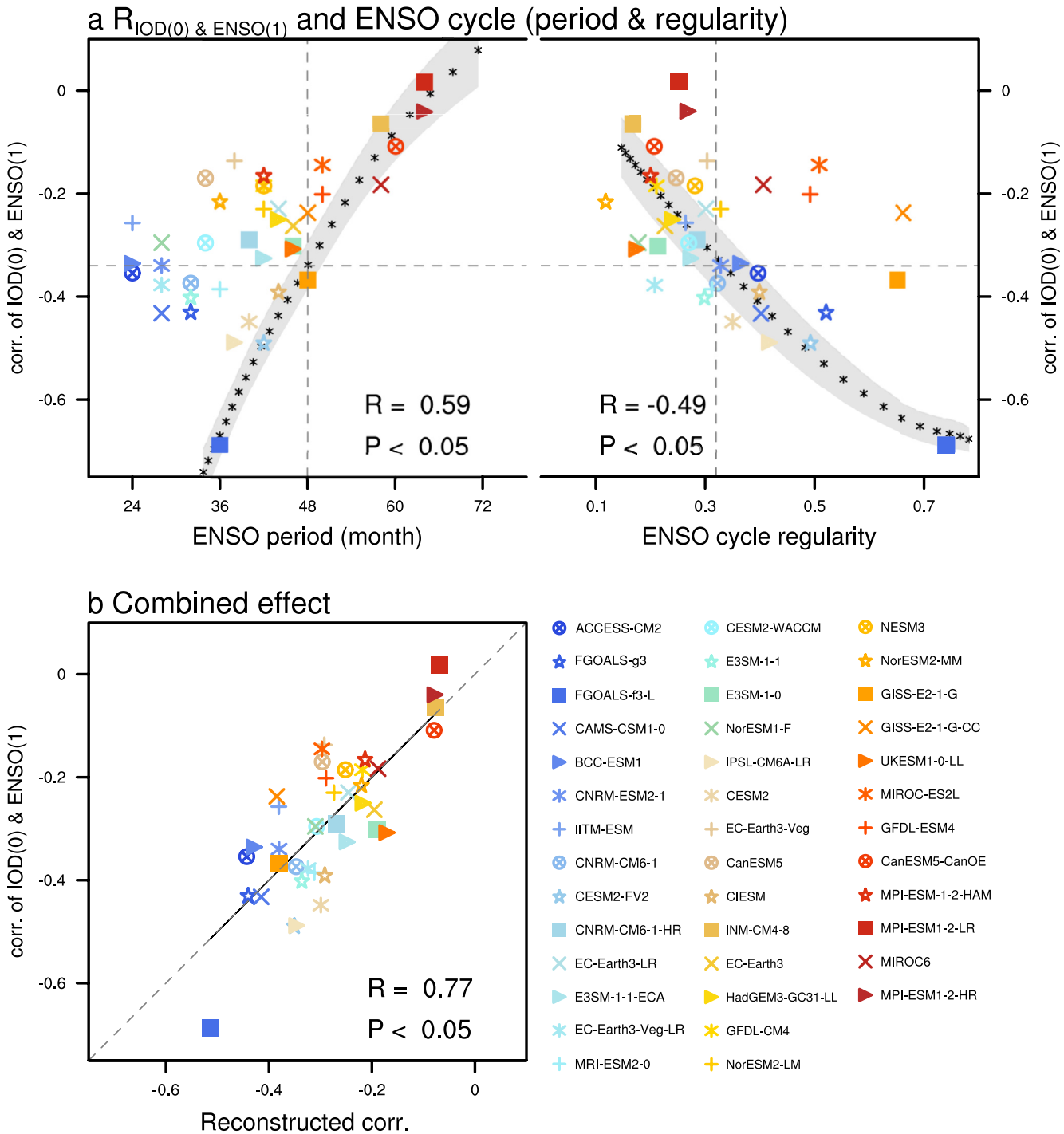

Figure 4. Factors regulating the statistical lead relationship of Indian Ocean dipole (IOD) over the following year El Niño-Southern Oscillation (ENSO) in pi-control climate simulations. (a) Scatterplot of correlation coefficients between the winter Niño3.4 index and autumn DMI of the previous year with ENSO period and ENSO cycle regularity. The black markers denote the relationship of correlation coefficients between the winter Niño3.4 index and autumn DMI of the previous year with ENSO period and ENSO cycle regularity in RO ENSO-IOD model experiments (see details in Section 2), superimposed by one standard deviation (gray shading). The gray dashed lines denote the observed ENSO period, ENSO cycle regularity, and statistical IOD lead relationship over ENSO. (b) Combined effect of ENSO period and its cycle regularity in determining the statistical IOD lead relationship with ENSO. Respective correlation coefficient *R* and *P* values are displayed in panels (a) and (b). The linear fit (solid black) is also shown in panel (b).

A more complicated and realistic perspective is that ENSO periodicity and regularity vary at the same time for different states of the climate system (Figures S2 and S3 in Supporting Information S1). These two factors are not correlated across the CMIP6 models ($R = -0.02$, statistically insignificant at the 95% confidence level), which makes the CMIP6 results less comparable to the theoretical experiments with controlled parameters (Figure 4a). Despite that, the qualitative relationship between the IOD-ENSO lead relationship with ENSO period and regularity can be well captured. A high inter-model relationship can be obtained ($R = 0.77$, exceeding the 95% confidence level) when considering these both factors (Figure 4c).

5. Conclusions

We have come to appreciate that ENSO provides a large fraction of seasonal climate predictability and successful ENSO forecasts therefore allow decision makers to improve climatic risk management (Pfaff et al., 1999). Despite significant advances in our understanding and simulation of ENSO, the ENSO predictions passing through the boreal spring are still of relatively low reliability and ENSO predictability has varied considerably from one decade to another (Allan et al., 1996; Latif et al., 1998; McPhaden, 2012; Zhang et al., 2019). Sustained efforts during recent years have largely paid off to find possible additional predictability sources outside of the tropical Pacific to potentially extend the prediction horizon of ENSO. However, we put forward a new concept here that the observed IOD-ENSO inter-basin lead-lag relationship is only a manifestation of ENSO cycle complexity, which is of crucial relevance for investigating inter-basin climate feedbacks. We emphasize that the character of the observed cross correlation between ENSO and IOD is tightly regulated by ENSO pacing. That is, the previously identified long-lead IOD signal actually adds no additional information to ENSO prediction despite that the possible feedback from IOD on ENSO is not quantified here. Therefore, to improve ENSO prediction skill, we need to refocus on tropical Pacific air-sea coupled dynamics (Zhang et al., 2021), particularly for understanding ENSO complexity and diversity (Timmermann et al., 2018) and improving climate models in their ability to simulate different ENSO types based on the right balance of feedback mechanisms (Hayashi et al., 2020).

Data Availability Statement

The data used to reproduce the results of this study are available online. Met Office Hadley Centre SST data are publicly available at: https://www.metoffice.gov.uk/hadobs/hadisst/data/download.html. The CMIP6 datasets are available at https://esgf-node.llnl.gov/projects/cmip6/.

Acknowledgments
This work was supported by the National Nature Science Foundation of China (42088101, 42125501) and the National Key Research and Development Program (2018YFC1506002). M. F. Stuecker was supported by NOAA's Climate Program Office's Modeling, Analysis, Predictions, and Projections (MAPP) Program grant NA20OAR4310445 and participates in the MAPP Marine Ecosystem Task Force. R. Allan is supported by funding from the U.K. Newton Fund under its CSSP China and WCSSP South Africa projects, plus the EU Copernicus C3S Data Rescue Service. This is IPRC publication 1537 and SOEST contribution 11408. The authors thank Axel Timmermann for valuable discussions.

References

Allan, R. J., Chambers, D., Drosdowsky, W., Hendon, H., & Tourre, Y. (2001). Is there an Indian Ocean dipole and is it independent of the El Niño-Southern Oscillation? *CLIVAR Exchanges*, *6*, 18–22.

Allan, R. J., Lindesay, J., & Parker, D. (1996). *El Niño Southern Oscillation & climatic variability*. Collingwood, Victoria, Australia: CSIRO Publishing.

Annamalai, H., Kida, S., & Hafner, J. (2010). Potential impact of the tropical Indian Ocean-Indonesian Seas on El Niño characteristics. *Journal of Climate*, *23*(14), 3933–3952. https://doi.org/10.1175/2010jcli3396.1

Annamalai, H., Murtugudde, R., Potemra, J., Xie, S. P., Liu, P., & Wang, B. (2003). Coupled dynamics over the Indian Ocean: Spring initiation of the zonal mode. *Deep Sea Research*, *50*(12–13), 2305–2330. https://doi.org/10.1016/s0967-0645(03)00058-4

Battisti, D. S. (1988). Dynamics and thermodynamics of a warming event in a coupled tropical atmosphere-ocean model. *Journal of the Atmospheric Sciences*, *45*(20), 2889–2919. https://doi.org/10.1175/1520-0469(1988)045<2889:datoaw>2.0.co;2

Behera, S. K., Luo, J.-J., Masson, S., Rao, S. A., Sakuma, H., & Yamagata, T. (2006). A CGCM study on the interaction between IOD and ENSO. *Journal of Climate*, *19*(9), 1688–1705. https://doi.org/10.1175/jcli3797.1

Cai, W., Wu, L., Lengaigne, M., Li, T., Mcgregor, S., Kug, J.-S., et al. (2019). Pantropical climate interactions. *Science*, *363*, eaav4236. https://doi.org/10.1126/science.aav4236

Cane, M. A., & Zebiak, S. E. (1985). A theory for El Niño and the Southern Oscillation. *Science*, *228*, 1085–1087. https://doi.org/10.1126/science.228.4703.1085

Chen, H. C., & Jin, F.-F. (2020). Fundamental behavior of ENSO phase locking. *Journal of Climate*, *33*(5), 1953–1968. https://doi.org/10.1175/jcli-d-19-0264.1

Clarke, A. J., & Van Gorder, S. (2003). Improving El Niño prediction using a space-time integration of Indo-Pacific winds and equatorial Pacific upper ocean heat content. *Geophysical Research Letters*, *30*, 1399. https://doi.org/10.1029/2002gl016673

Dommenget, D., & Latif, M. (2002). A cautionary note on the interpretation of EOFs. *Journal of Climate*, *15*(2), 216–225. https://doi.org/10.1175/1520-0442(2002)015<0216:acnoti>2.0.co;2

Dommenget, D., Semenov, V., & Latif, M. (2006). Impacts of the tropical Indian and Atlantic Oceans on ENSO. *Geophysical Research Letters*, *33*, L11701. https://doi.org/10.1029/2006gl025871

Frauen, C., & Dommenget, D. (2012). Influences of the tropical Indian and Atlantic Oceans on the predictability of ENSO. *Geophysical Research Letters*, *39*, L02706. https://doi.org/10.1029/2011gl050520
Hasselmann, K. (1976). Stochastic climate models, Part I. Theory. *Tellus*, *28*(6), 473–485. https://doi.org/10.3402/tellusa.v28i6.11316
Hayashi, M., Jin, F.-F., & Stuecker, M. F. (2020). Dynamics for El Niño-La Niña asymmetry constrain equatorial-Pacific warming pattern. *Nature Communications*, *11*(1), 1–10. https://doi.org/10.1038/s41467-020-17983-y
Hendon, H. H., Lim, E., Wang, G., Alves, O., & Hudson, D. (2009). Prospects for predicting two flavors of El Niño. *Geophysical Research Letters*, *36*, L19713. https://doi.org/10.1029/2009gl040100
Izumo, T., Lengaigne, M., Vialard, J., Luo, J. J., Yamagata, T., & Madec, G. (2014). Influence of Indian Ocean Dipole and Pacific recharge on following year's El Niño: Interdecadal robustness. *Climate Dynamics*, *42*(1–2), 291–310. https://doi.org/10.1007/s00382-012-1628-1
Izumo, T., Vialard, J., Lengaigne, M., Montegut, C. D. B., Yamagata, T., Luo, J.-J., et al. (2010). Influence of the state of the Indian Ocean Dipole on the following year's El Niño. *Nature Geoscience*, *3*(3), 168–172. https://doi.org/10.1038/ngeo760
Jansen, M. F., Dommenget, D., & Keenlyside, N. (2009). Tropical atmosphere-ocean interactions in a conceptual framework. *Journal of Climate*, *22*(3), 550–567. https://doi.org/10.1175/2008jcli2243.1
Jin, F.-F. (1997a). An equatorial ocean recharge paradigm for ENSO. Part I: Conceptual model. *Journal of the Atmospheric Sciences*, *54*(7), 811–829. https://doi.org/10.1175/1520-0469(1997)054<0811:aeorpf>2.0.co;2
Jin, F.-F. (1997b). An equatorial recharge paradigm for ENSO: II. A stripped-down coupled model. *Journal of the Atmospheric Sciences*, *54*(7), 830–847. https://doi.org/10.1175/1520-0469(1997)054<0830:aeorpf>2.0.co;2
Kajtar, J. B., Santoso, A., England, M. H., & Cai, W. (2017). Tropical climate variability: Interactions across the Pacific, Indian, and Atlantic Oceans. *Climate Dynamics*, *48*(7–8), 2173–2190. https://doi.org/10.1007/s00382-016-3199-z
Kug, J.-S., An, S.-I., Jin, F.-F., & Kang, I.-S. (2005). Preconditions for El Niño and La Niña onsets and their relation to the Indian Ocean. *Geophysical Research Letters*, *32*, L05706. https://doi.org/10.1029/2004gl021674
Kug, J.-S., & Kang, I.-S. (2006). Interactive feedback between ENSO and the Indian Ocean. *Journal of Climate*, *19*(9), 1784–1801. https://doi.org/10.1175/jcli3660.1
Latif, M., Anderson, D., Barnett, T., Cane, M., Kleeman, R., Leetmaa, A., et al. (1998). A review of the predictability and prediction of ENSO. *Journal of Geophysical Research: Oceans*, *103*(C7), 14375–14393. https://doi.org/10.1029/97jc03413
Luo, J.-J., Zhang, R., Behera, S. K., Masumoto, Y., Jin, F.-F., Lukas, R., & Yamagata, T. (2010). Interaction between El Nino and extreme Indian Ocean Dipole. *Journal of Climate*, *23*(3), 726–742. https://doi.org/10.1175/2009jcli3104.1
McPhaden, M. J. (2012). A 21st century shift in the relationship between ENSO SST and warm water volume anomalies. *Geophysical Research Letters*, *39*, L09706. https://doi.org/10.1029/2012gl051826
McPhaden, M. J., Zebiak, S. E., & Glantz, M. H. (2006). ENSO as an integrating concept in earth science. *Science*, *314*(5806), 1740–1745. https://doi.org/10.1126/science.1132588
Meinen, C. S., & McPhaden, M. J. (2000). Observations of warm water volume changes in the equatorial Pacific and their relationship to El Niño and La Niña. *Journal of Climate*, *13*(20), 3551–3559. https://doi.org/10.1175/1520-0442(2000)013<3551:oowwvc>2.0.co;2
Pfaff, A., Broad, K., & Glantz, M. (1999). Who benefits from climate forecasts? *Nature*, *397*(6721), 645–646. https://doi.org/10.1038/17676
Quinn, W. (1974). Monitoring and predicting El Niño invasions. *Journal of Applied Meteorology*, *13*(7), 825–830. https://doi.org/10.1175/1520-0450(1974)013<0825:mapeni>2.0.co;2
Rayner, N. A. A., Parker, D. E., Horton, E. B., Folland, C. K., Alexander, L. V., Rowell, D. P., et al. (2003). Global analyses of sea surface temperature, sea ice, and night marine air temperature since the late nineteenth century. *Journal of Geophysical Research*, *108*, 4407. https://doi.org/10.1029/2002jd002670
Saji, N. H., Goswami, B. N., Vinayachandran, P. N., & Yamagata, T. (1999). A dipole mode in the tropical Indian Ocean. *Nature*, *401*(6751), 360–363. https://doi.org/10.1038/43854
Stuecker, M. F., Timmermann, A., Jin, F.-F., Chikamoto, Y., Zhang, W., Wittenberg, A. T., et al. (2017). Revisiting ENSO/Indian Ocean dipole phase relationships. *Geophysical Research Letters*, *44*(5), 2481–2492. https://doi.org/10.1002/2016gl072308
Sun, S., Lan, J., Fang, Y., Gao, X., & Gao, X. (2015). A triggering mechanism for the Indian Ocean dipoles independent of ENSO. *Journal of Climate*, *28*(13), 5063–5076. https://doi.org/10.1175/jcli-d-14-00580.1
Thomson, D. J. (1982). Spectrum estimation and harmonic analysis. *Proceedings of the IEEE*, *70*(9), 1055–1096. https://doi.org/10.1109/proc.1982.12433
Timmermann, A., An, S. I., Kug, J.-S., Jin, F.-F., Cai, W., Capotondi, A., et al. (2018). El Niño-Southern Oscillation complexity. *Nature*, *559*(7715), 535–545. https://doi.org/10.1038/s41586-018-0252-6
Wang, C. (2019). Three-ocean interactions and climate variability: A review and perspective. *Climate Dynamics*, *53*(7), 5119–5136. https://doi.org/10.1007/s00382-019-04930-x
Wang, W., Chen, M., & Kumar, A. (2010). An assessment of the CFS real-time seasonal forecasts. *Weather and Forecasting*, *25*(3), 950–969. https://doi.org/10.1175/2010waf2222345.1
Webster, P. J., Moore, A. M., Loschnigg, J. P., & Leben, R. R. (1999). Coupled oceanic-atmospheric dynamics in the Indian Ocean during 1997–98. *Nature*, *401*, 356–360. https://doi.org/10.1038/43848
Webster, P. J., & Yang, S. (1992). Monsoon and ENSO: Selectively interactive systems. *Quarterly Journal of the Royal Meteorological Society*, *118*(507), 877–926. https://doi.org/10.1002/qj.49711850705
Wu, R., & Kirtman, B. P. (2004). Understanding the impacts of the Indian Ocean on ENSO variability in a coupled GCM. *Journal of Climate*, *17*, 4019–4031. https://doi.org/10.1175/1520-0442(2004)017<4019:utioti>2.0.co;2
Wyrtki, K. (1975). El Niño—the dynamic response of the equatorial Pacific Ocean to atmospheric forcing. *Journal of Physical Oceanography*, *5*(4), 572–584. https://doi.org/10.1175/1520-0485(1975)005<0572:entdro>2.0.co;2
Wyrtki, K., Stroup, E., Patzert, W., Williams, R., & Quinn, W. (1976). Predicting and observing El Niño. *Science*, *191*(4225), 343–346. https://doi.org/10.1126/science.191.4225.343
Xie, S. P., Hu, K., Hafner, J., Tokinaga, H., Du, Y., Huang, G., & Sampe, T. (2009). Indian Ocean capacitor effect on Indo-Western Pacific climate during the summer following El Niño. *Journal of Climate*, *22*(3), 730–747. https://doi.org/10.1175/2008jcli2544.1
Yang, J., Liu, Q., Xie, S. P., Liu, Z., & Wu, L. (2007). Impact of the Indian Ocean SST basin mode on the Asian summer monsoon. *Geophysical Research Letters*, *34*, L02708. https://doi.org/10.1029/2006gl028571
Yang, Y., Xie, S. P., Wu, L., Kosaka, Y., Lau, N. C., & Vecchi, G. A. (2015). Seasonality and predictability of the Indian Ocean dipole mode: ENSO forcing and internal variability. *Journal of Climate*, *28*(20), 8021–8036. https://doi.org/10.1175/jcli-d-15-0078.1
Yu, J. Y., Mechoso, C. R., McWilliams, J. C., & Arakawa, A. (2002). Impacts of the Indian Ocean on the ENSO cycle. *Geophysical Research Letters*, *29*(8), 46-1–46-4. https://doi.org/10.1029/2001gl014098

Zebiak, S. E., & Cane, M. A. (1987). A model El Niño-Southern Oscillation. *Monthly Weather Review*, *115*(10), 2262–2278. https://doi.org/10.1175/1520-0493(1987)115<2262:ameno>2.0.co;2

Zhang, W., Jiang, F., Stuecker, M. F., Jin, F.-F., & Timmermann, A. (2021). Spurious North Tropical Atlantic precursors to El Niño. *Nature Communications*, *12*(1), 1–8. https://doi.org/10.1038/s41467-021-23411-6

Zhang, W., Li, S., Jin, F.-F., Xie, R., Liu, C., Stuecker, M. F., & Xue, A. (2019). ENSO regime changes responsible for decadal phase relationship variations between ENSO sea surface temperature and warm water volume. *Geophysical Research Letters*, *46*(13), 7546–7553. https://doi.org/10.1029/2019gl082943

Zhao, S., Jin, F.-F., & Stuecker, M. F. (2019). Improved predictability of the Indian Ocean dipole using seasonally modulated ENSO forcing forecasts. *Geophysical Research Letters*, *46*(16), 9980–9990. https://doi.org/10.1029/2019gl084196

Zhao, S., Stuecker, M. F., Jin, F.-F., Feng, J., Ren, H. L., Zhang, W., & Li, J. (2020). Improved predictability of the Indian Ocean Dipole using a stochastic dynamical model compared to the North American multimodel ensemble forecast. *Weather and Forecasting*, *35*(2), 379–399. https://doi.org/10.1175/waf-d-19-0184.1

References From the Supporting Information

An, S.-I. (2008). Interannual variations of the tropical ocean instability wave and ENSO. *Journal of Climate*, *21*(15), 3680–3686. https://doi.org/10.1175/2008jcli1701.1

Boucharel, J., & Jin, F.-F. (2020). A simple theory for the modulation of tropical instability waves by ENSO and the annual cycle. *Tellus A: Dynamic Meteorology and Oceanography*, *72*(1), 1–14. https://doi.org/10.1080/16000870.2019.1700087

Burgers, G., Jin, F.-F., & Van Oldenborgh, G. J. (2005). The simplest ENSO recharge oscillator. *Geophysical Research Letters*, *32*, L13706. https://doi.org/10.1029/2005gl022951

Frankignoul, C., & Hasselmann, K. (1977). Stochastic climate models, Part II Application to sea-surface temperature anomalies and thermocline variability. *Tellus*, *29*(4), 289–305. https://doi.org/10.3402/tellusa.v29i4.11362

Jin, F.-F., Kim, S. T., & Bejarano, L. (2006). A coupled-stability index for ENSO. *Geophysical Research Letters*, *33*, L23708. https://doi.org/10.1029/2006gl027221

Jin, F.-F., Lin, L., Timmermann, A., & Zhao, J. (2007). Ensemble–mean dynamics of the ENSO recharge oscillator under state-dependent stochastic forcing. *Geophysical Research Letters*, *34*, L03807. https://doi.org/10.1029/2006gl027372

Levine, A. F., & Jin, F.-F. (2010). Noise-induced instability in the ENSO recharge oscillator. *Journal of the Atmospheric Sciences*, *67*(2), 529–542. https://doi.org/10.1175/2009jas3213.1

Lu, B., Jin, F.-F., & Ren, H. L. (2018). A coupled dynamic index for ENSO periodicity. *Journal of Climate*, *31*(6), 2361–2376. https://doi.org/10.1175/jcli-d-17-0466.1